Original Article

Institution of MECHANICAL ENGINEERS

Journal of AUTOMOBILE ENGINEERING

Proc IMechE Part D:
J Automobile Engineering
226(11) 1454–1471

DOI: 10.1177/0954407012445698
pid.sagepub.com
SAGE

The influence of a vehicle dynamics control system on the occupant's dynamic response during a vehicle collision

Mustafa Elkady[1,2], Ahmed Elmarakbi[1] and John MacIntyre[1]

Abstract

This paper aims to apply a vehicle dynamics control system to mitigate a vehicle collision and to study the effects of this systems on the kinematic behaviour of the vehicle's occupant. A unique three-degree-of-freedom vehicle dynamics–crash mathematical model and a simplified lumped-mass occupant model are developed. The first model is used to define the vehicle body's crash parameters and it integrates a vehicle dynamics model with a model of the vehicle's front-end structure. In this model, the anti-lock braking system and the active suspension control system are co-simulated, and the associated equations of motion are developed. The second model aims to predict the effect of the vehicle dynamics control system on the kinematics of the occupant. The Lagrange equations are used to solve that model owing to the complexity of the obtained equations of motion. It is shown from the numerical simulations that the vehicle dynamics–crash response and occupant behaviour can be captured and analysed quickly and accurately. Furthermore, it is shown that the vehicle dynamics control system can affect the crash characteristics positively and that the occupant's behaviour is improved.

Keywords

Active safety, collision mitigation, vehicle dynamics, vehicle control, mathematical modelling, numerical simulations, occupant kinematics

Date received: 21 December 2011; accepted: 23 March 2012

Introduction

Nowadays, occupant safety is an important subject in the automotive research and industry. Seat belts, air bags and advanced driver assistance systems (ADASs) have been developed to prevent a vehicle crash or to mitigate vehicle collision when an accident occurs. Furthermore, to improve the vehicle crash energy absorption capability, the vehicle's front-end and side structures have been developed and enhanced.

ADAS techniques have been investigated in an endeavour to alleviate vehicle crashes.[1–5] The main purpose of the ADAS is to warn the driver of dangerous situations and to provide active aid in an impending collision. However, ADASs have yet to achieve their goal of preventing vehicle collisions.

In terms of the absorption of crash energy, two types of smart front-end structure were proposed to mitigate vehicle-to-vehicle frontal collisions;[6–9] they consist of two hydraulic cylinders integrated with the front-end longitudinal members of conventional vehicles. Two mathematical models have been developed: one to represent the vehicle and its associated smart front-end structure, and the other to represent the occupant. Both models use lumped masses and spring–damper systems. It was demonstrated from these studies that intrusions and decelerations were reduced.

With regard to the occupant safety, vehicle body pitch and drop during frontal impact play important roles in a driver's neck and head injuries.[10–12] Vehicle body pitch and drop have normally been experienced in frontal crash tests. Chang et al.[10] used a finite

[1]Department of Computing, Engineering and Technology, University of Sunderland, Sunderland, UK
[2]Department of Automotive Engineering, Ain Shams University, Cairo, Egypt

Corresponding author:
Musatafa Elkady, Department of Computing, Engineering and Technology, University of Sunderland, The Sir Tom Cowie Campus at St Peter's, St Peter's Way, Sunderland SR6 0DD, UK.
Email: ahmed.elmarakbi@sunderland.ac.uk

element method to investigate frame deformation upon full-frontal impact and discussed the cause and countermeasures design regarding vehicle body pitch and drop. It was found that downward bending generated from the geometric offsets of the frame rails in the vertical direction during a crash is the key feature of the pitching of the vehicle body.

The development of a vehicle dynamics control system (VDCS) plays an important role in improving the stability, ride characteristics and passenger safety of a vehicle. The anti-lock braking system (ABS) and the yaw moment control system are used to help vehicle stability during emergency manoeuvres, while the active suspension (AS) control system is used to improve the vehicle ride quality and to reduce the vertical acceleration of the vehicle.[13,14] In addition, the AS control system integrated with the ABS is used to reduce the vehicle's stopping distance.[15]

Few researchers have investigated the effect of a VDCS on vehicle crashworthiness and collision mitigation. The influence of the braking force on the impact dynamics of a vehicle in low-speed rear-end collisions was studied[16] and this confirmed that the braking force was not negligible in high-quality simulations of the vehicle's impact dynamics at low speeds. The effects of vehicle braking and anti-pitch control systems on the crash routine have been investigated by Hogan and Manning,[17] who also investigated the possibility of using a VDCS to improve the vehicle collision performance in frontal and offset vehicle-to-barrier collisions. The ADAMS multi-body model was used to simulate the characteristics of the vehicle structure together with the vehicle dynamics. In this study the anti-pitch control system was minimally involved and the crash pulse was affected by the braking force; however, more research into the effects of the braking and anti-pitch control systems was recommended. Further research focused on vehicle compatibility; the effect of a VDCS on vehicle-to-barrier offset collisions[18,19] and vehicle-to-vehicle offset collisions[19] was studied. It was found that the VDCS had different levels of effectiveness depending on the collision scenario.

Mathematical modelling

The frontal collision of a vehicle can be divided into two main stages: the first is a primary impact, and the second is a secondary impact. The primary impact indicates the collision between the front-end structure of the vehicle and an obstacle (a barrier in this paper). The secondary impact is the interaction between the occupant and the restraint system and/or the vehicle interior due to vehicle collisions.

Vehicle dynamics–crash model

Using mathematical models in a crash simulation is useful for the first design concept because rapid analysis is required at this stage.[20–22] In addition, the well-known advantage of mathematical modelling provides a quick simulation analysis compared with finite-element models.

A three-degree-of-freedom (3-DOF) vehicle dynamics–crash mathematical model was developed to study the effect of a VDCS on vehicle collision mitigation. Full-frontal vehicle-to-barrier crash scenarios are considered in this research. In this model, the vehicle body and the bumper are represented by lumped masses, and the front-end structure is represented by two springs (the upper and lower springs) with piecewise non-linear characteristics. The ABS and the AS control systems are co-simulated with a vehicle dynamic–crash mathematical model and integrated with a front-end crash model, as shown in Figure 1(a).

Figure 1(b) and (c) shows deformation of the front end and vehicle pitching at the early stage and at the end of impact respectively. At the first stage of impact, deformation of the front end and vehicle pitching are small while, at the end of impact, deformation of the front end reaches its maximum level, the vehicle pitch angle increases and the rear wheels leave the ground. It is worth noting that the rear wheels will leave the ground only in certain cases while the impact velocity is high. In our case, the impact velocity is sufficiently high that the wheels leave the road. It is assumed that the

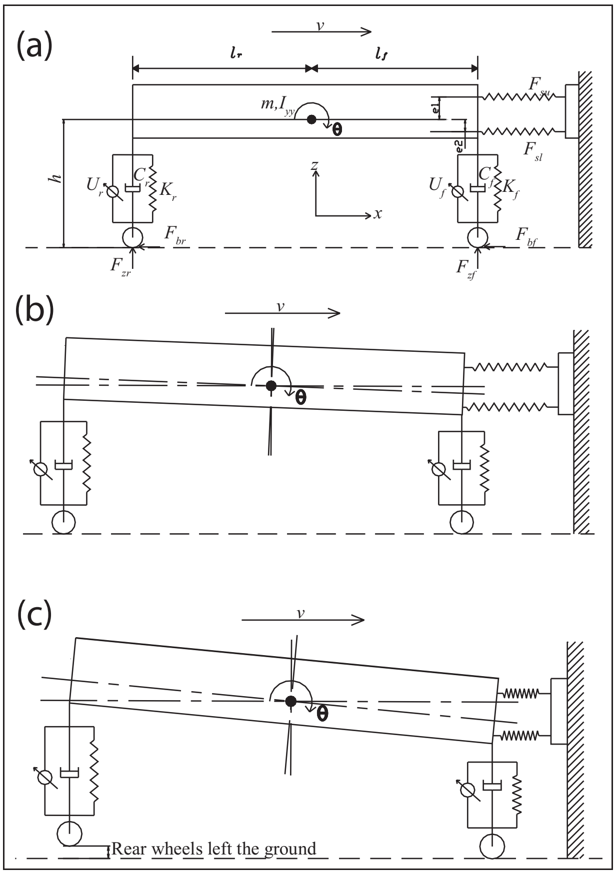

Figure 1. (a) Vehicle dynamics–crash mathematical model; (b) a schematic diagram showing the model at the early stage of the impact; (c) a schematic diagram showing the model at the end of impact.

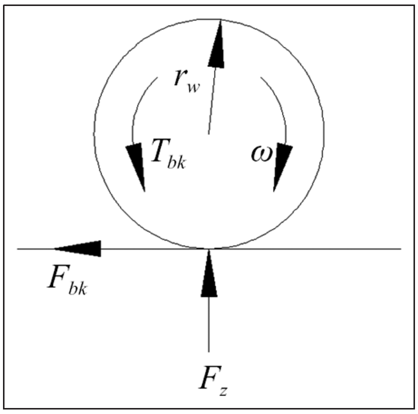

Figure 2. Wheel–road model.

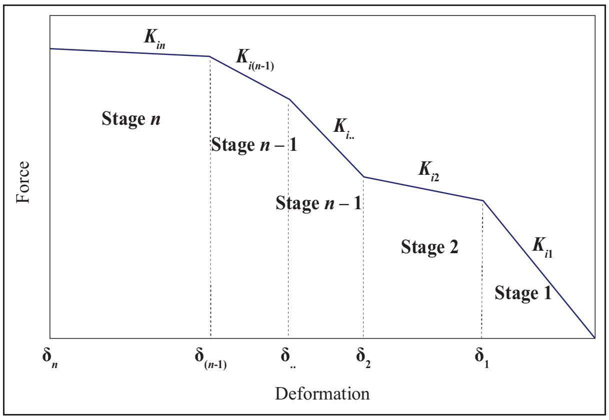

Figure 3. General piecewise force–deformation characteristics.

front-end springs are still horizontal during impact, and they will not incline with the vehicle body.

In this model, the vehicle body is represented by the lumped mass m, and two spring–damper units are used to represent the vehicle's suspension system. The mass of the bumper is neglected because of full contact of the bumper with the barrier. It is assumed that the vehicle moves on a flat asphalted road; thus the vertical movement of the tyres and the road vertical forces can be neglected. The ABS is co-simulated with the mathematical model using the simple wheel–road model shown in Figure 2, and its associated equations can be written as

$$I\dot{\omega} = F_{bk}r_w - T_{bk} \tag{1}$$

$$F_{bk} = \mu(\lambda)F_{zk} \tag{2}$$

where the slip ratio λ is defined as

$$\lambda = \frac{v - \omega r_w}{v} \tag{3a}$$

and the relationship between $\mu(\lambda)$ and the wheel slip λ can be determined from the equation

$$\mu(\lambda) = 2\mu_0 \frac{\lambda_0 \lambda}{\lambda_0^2 + \lambda^2} \tag{3b}$$

where I is the wheel's moment of inertia, ω is the wheel's angular velocity, $\dot{\omega}$ is the wheel's angular acceleration, r_w is the wheel's radius, T_b is the braking torque applied by the disc and/or drum brakes, μ is the friction coefficient between the tyre and the road, λ is the tyre slip ratio, F_z is the vertical normal forces of the tyres and v is the velocity of the vehicle body. The subscript k indicates the wheel's location (where $k = f$ indicates the front wheel and $k = r$ indicates the rear wheel). The slip ratio λ can be estimated using the wheel model discussed above. Relating to the values of λ, the ABS controller turns the brake on and off to sustain μ at its maximum values; therefore the maximum braking force can be obtained. At the beginning, the ABS controller turns on and the braking torque is applied while the slip ratio λ is equal to 0. When the slip ratio λ reaches 0.3, the ABS controller turns off, causing a reduction in the slip ratio value. Finally, when the slip ratio reaches 0.18, the ABS controller is turned on and the slip ratio increases again; this process is repeated during the braking time.

The vertical forces F_{zk} at each wheel can be written as

$$F_{zf} = mg\frac{l_r}{l} + F_{Sf} \tag{4}$$

$$F_{zr} = mg\frac{l_f}{l} + F_{Sr} \tag{5}$$

where m is the mass of the vehicle body and g is the acceleration due to gravity. l_f, l_r and l represent the longitudinal distance between the vehicle's centre of gravity (CG) and the front wheels, the longitudinal distance between the CG and the rear wheels and the wheelbase respectively, and F_S represents the suspension force. The subscripts f and r denote the front vehicle wheels and the rear vehicle wheels respectively. The suspension forces can also be written as

$$F_{Sf} = k_{Sf}(z - l_f \sin\theta) + c_f(\dot{z} - l_f\dot{\theta}\cos\theta) - u_f \tag{6}$$

$$F_{Sr} = k_{Sr}(z + l_r \sin\theta) + c_r(\dot{z} + l_r\dot{\theta}\cos\theta) - u_r \tag{7}$$

where k_S, c and u represent the stiffness of the suspension springs, the damping of the suspension coefficients and the active suspension force elements respectively. z and θ are the vertical displacement and the pitch angle of the vehicle body respectively. $\dot{z}$ and $\dot{\theta}$ are the velocity in the vertical direction and the pitch angular velocity of the vehicle body respectively.

The AS is simulated, and its force elements are taken to be 2000 N for each wheel in the upward direction with the maximum suspension travel limit of 100 mm considering the response time of the AS system.[15]

A general multi-stage force–deformation curve with piecewise non-linear characteristics could be considered to simulate the front-end springs, as shown in Figure 3. In this paper, to simulate the upper and lower springs, the force–deformation curves used in the multi-body model[19] are used to generate the n-stage piecewise spring's characteristics, as shown in Figure 4. It is assumed that the spring force is deactivated after small restitution to represent plastic deformation of the

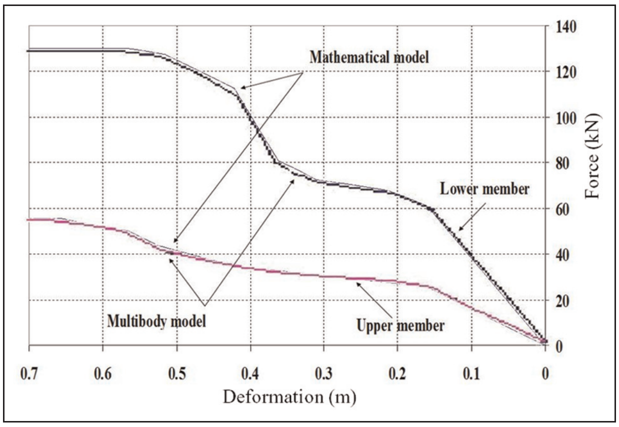

Figure 4. Force–deformation characteristics for the upper and lower rails.

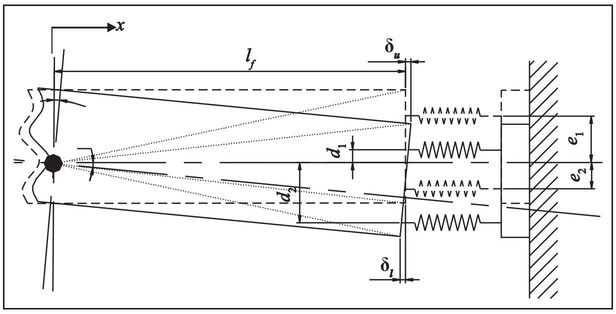

Figure 5. A schematic diagram showing the deformation of the front-end structure due to the vehicle pitching: – – –, before pitching; ——, after pitching.

front-end structure. The forces of the non-linear springs shown in Figure 3 are defined using piecewise functions in the displacement domain which are given by

$$F_{si} = k_{sij}\delta_i + F_{ij} \tag{8a}$$

where F_s is the front-end spring force and where k_s, δ and F represent the stiffness, deflection and force elements of the front-end spring respectively. The subscript i indicates the spring location ($i = u$ indicates the upper springs and $i = l$ indicates the lower springs) and the subscript j indicates different stages of the force–deformation characteristics, as shown in Figure 3. The stiffness k_s of the spring and the force elements F_{ij} vary according to the different stages of the deflection δ and can be defined as

$$k_{sij} = k_{si1}, \quad F_{ij} = 0, \qquad 0 \leqslant \delta < \delta_{i1} \tag{8b}$$

$$k_{sij} = k_{si2}, \quad F_{ij} = (k_{si1} - k_{si2})\delta_{i1}, \quad \delta_{i1} \leqslant \delta < \delta_{i2} \tag{8c}$$

$$k_{sij} = k_{si3}, \quad F_{ij} = (k_{si1} - k_{si2})\delta_{i1} + (k_{si2} - k_{si3})\delta_{i2}, \quad \delta_{i2} \leqslant \delta < \delta_{i3} \tag{8d}$$

$$k_{sij} = k_{\sin}, \quad F_{ij} = (k_{si1} - k_{si2})\delta_{i1} + (k_{si2} - k_{si3})\delta_{i2} + \cdots + (k_{si(n-1)} - k_{\sin})\delta_{i(n-1)}, \quad \delta \geqslant \delta_{(n-1)} \tag{8e}$$

where the deformations δ_i of the front-end springs can be calculated for the upper and lower springs using Figure 5 as

$$\delta_u = x + \sqrt{l_f^2 + e_1^2}\cos\left[\tan^{-1}\left(\frac{e_1}{l_f}\right) - \theta\right] - l_f \tag{9a}$$

$$\delta_l = x - \sqrt{l_f^2 + e_2^2}\cos\left[\tan^{-1}\left(\frac{e_2}{l_f}\right) + \theta\right] + l_f \tag{9b}$$

where x represents the longitudinal displacement of the vehicle body, and e_1 and e_2 represent the distance between the CG and the upper springs and the distance between the CG and the lower springs respectively.

The equations of motion of the mathematical model can be written as

$$m\ddot{x} + F_{su} + F_{sl} + F_{bf} + F_{br} = 0 \tag{10}$$

$$m\ddot{z} + F_{Sf} + F_{Sr} = 0 \tag{11}$$

$$I_{yy}\ddot{\theta} - F_{Sf}l_f + F_{Sr}l_r + F_{su}d_1 - F_{sl}d_2 - (F_{bf} + F_{br})(z + h) = 0 \tag{12}$$

where I_{yy} is the moment of inertia of the vehicle body about the y axis, $\ddot{x}$ is the acceleration of the vehicle body in the longitudinal direction, $\ddot{z}$ is the acceleration of the vehicle body in the vertical direction, $\ddot{\theta}$ is the rotational pitch acceleration of the vehicle body and h is the CG height from ground. d_1 and d_2 represent the distance between the CG and the force of the upper springs and the distance between the CG and the force of the lower springs respectively, and they can be calculated, using Figure 5, as

$$d_1 = \sqrt{l_f^2 + e_1^2}\sin\left[\tan^{-1}\left(\frac{e_1}{l_f}\right) - \theta\right] \tag{13}$$

$$d_2 = \sqrt{l_f^2 + e_2^2}\sin\left[\tan^{-1}\left(\frac{e_2}{l_f}\right) + \theta\right] \tag{14}$$

The model's equations are solved using the central difference method.

Multi-body occupant model

There are many techniques for occupant modelling such as finite element modelling[23] and MADYMO software modelling.[24] In our study, the occupant is modelled mathematically to be integrated with the above mathematical model of the vehicle. The occupant can be modelled as a one-mass model,[6–9] a two-mass model,[25,26] a three-mass model[27,28] or a multi-mass model.[29] In most of these previous studies, the researchers claimed that simple occupant mathematical models can obtain usefully similar results to sophisticated analytical and experimental work.

The occupant mathematical model shown in Figure 6(a) is developed to evaluate the occupant's kinematic behaviour in full-frontal crash scenarios. The human body model consists of three bodies, with masses m_1, m_2 and m_3.[27] The first body (i.e. the lower body), with mass m_1, represents the legs and the pelvic area of the occupant and is considered to have a translation motion in the longitudinal direction and a rotation motion around the CG of the vehicle. The second body (i.e. the middle body), with mass m_2, represents the occupant's abdominal area, the thorax area and the arms and is considered to have a translation motion in the longitudinal direction and rotation motion around the pivot between the lower and middle bodies (pivot 1). The third body (i.e. the upper body), with mass m_3, represents the head and neck of the occupant and is considered to have a translation motion in the longitudinal direction and rotation motion around the pivot between the middle body and the upper body (pivot 2). Two rotational springs are considered at each pivot to represent the joint stiffness, namely between the pelvic area and the abdominal area and between the thorax area and the neck–head area respectively. The seat belt is represented by two linear spring–damper units between the compartment and the occupant. Figure 6(b) shows the vehicle body and the occupant behaviours at the end of impact. At this point the lower body moves forwards and reaches its maximum position, while the middle and upper bodies start to rotate, although they have not reached their maximum position yet.

The equation of motion of the human body, using Lagrange's method, is generated as

$$\frac{\mathrm{d}}{\mathrm{d}t}\left(\frac{\partial E}{\partial \dot{x}_1}\right) - \frac{\partial E}{\partial x_1} + \frac{\partial V}{\partial x_1} + \frac{\partial D}{\partial \dot{x}_1} = 0 \tag{15a}$$

$$\frac{\mathrm{d}}{\mathrm{d}t}\left(\frac{\partial E}{\partial \dot{\theta}_2}\right) - \frac{\partial E}{\partial \theta_2} + \frac{\partial V}{\partial \theta_2} + \frac{\partial D}{\partial \dot{\theta}_2} = 0 \tag{15b}$$

$$\frac{\mathrm{d}}{\mathrm{d}t}\left(\frac{\partial E}{\partial \dot{\theta}_3}\right) - \frac{\partial E}{\partial \theta_3} + \frac{\partial V}{\partial \theta_3} + \frac{\partial D}{\partial \dot{\theta}_3} = 0 \tag{15c}$$

where E, V and D are the kinetic energy, the potential energy and the Rayleigh dissipation function respectively of the system. x_1, θ_2 and θ_3 are the longitudinal movement of the occupant's lower body, the rotation angle of the occupant's middle body and the rotation angle of the occupant's upper body respectively, and $\dot{x}_1$, $\dot{\theta}_2$ and $\dot{\theta}_3$ are the corresponding velocities. The rotation angles θ_2 and θ_3 are measured on the basis of their inclinations relative to the vertical position.

The kinetic energy of the system can be written as

$$E = \frac{m_1 v_1^2}{2} + \frac{m_2 v_2^2}{2} + \frac{m_3 v_3^2}{2} + \frac{I_1}{2}\dot{\theta}^2 + \frac{I_2}{2}\dot{\theta}_2^2 + \frac{I_3}{2}\dot{\theta}_3^2 \tag{16}$$

where v_1, v_2 and v_3 are the equivalent velocities of the lower body, the middle body and the upper body respectively of the occupant. I_1, I_2 and I_3 are the rotational moments of inertia of the lower body, the middle body and the upper body respectively about the CG of each body. The equivalent velocities of the three bodies of the occupant can be calculated as

$$v_1^2 = \dot{X}_{m_1}^2 + \dot{Y}_{m_1}^2 \tag{17a}$$

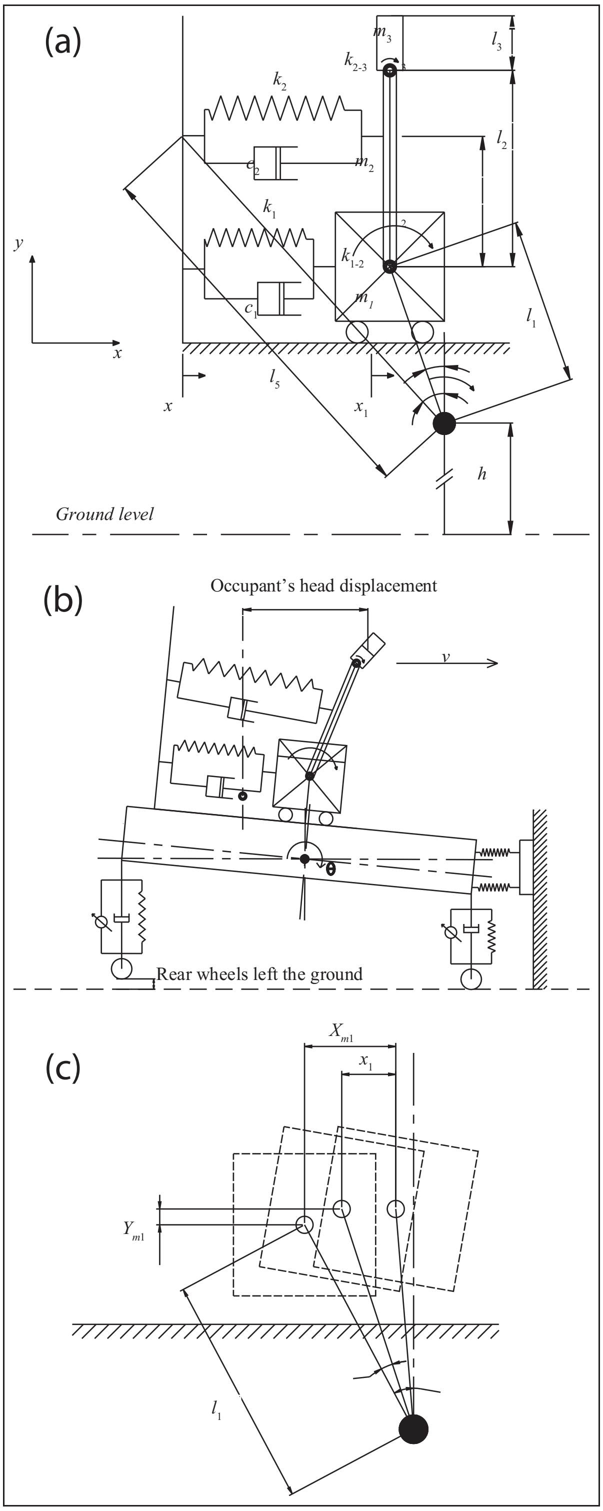

Figure 6. (a) Multi-body occupant model; (b) a schematic diagram of the vehicle and occupant at the end of impact; (c) a schematic diagram of the occupant's lower-body movement.

where the displacement and velocity of the lower body in the x direction can be calculated as

$$X_{m_1} = x_1 + l_1[\sin\beta - \sin(\beta - \theta)] \tag{17b}$$

$$\dot{X}_{m_1} = \dot{x}_1 + l_1\dot{\theta}\cos(\beta - \theta) \tag{17c}$$

and the displacement and velocity of the lower body in the y direction can be calculated as

$$Y_{m_1} = l_1[(\cos(\beta - \theta) - \cos\beta] \quad (17d)$$

$$\dot{Y}_{m_1} = l_1\dot{\theta}\sin(\beta - \theta) \quad (17e)$$

Substituting equations (17c) and (17e) in equation (17a), the equivalent velocity of the lower body can be written as

$$v_1^2 = \dot{x}_1^2 + l_1^2\dot{\theta}^2 + 2\dot{x}_1 l_1\dot{\theta}\cos(\beta - \theta) \quad (17f)$$

By repeating the previous steps of equation (17), the equivalent velocities of the middle body and the upper body can be calculated as

$$v_2^2 = \dot{X}_{m_2}^2 + \dot{Y}_{m_2}^2 \quad (18a)$$

$$X_{m_2} = x_1 + l_1[\sin\beta - \sin(\beta - \theta)] + \frac{l_2}{2}\sin\theta_2 \quad (18b)$$

$$\dot{X}_{m_2} = \dot{x}_1 + l_1\dot{\theta}\cos(\beta - \theta) + \frac{l_2}{2}\dot{\theta}_2\cos\theta_2 \quad (18c)$$

$$Y_{m_2} = l_1[\cos(\beta - \theta) - \cos\beta] - \frac{l_2}{2}(1 - \cos\theta_2) \quad (18d)$$

$$\dot{Y}_{m_2} = l_1\dot{\theta}\sin(\beta - \theta) - \frac{l_2}{2}\dot{\theta}_2\sin\theta_2 \quad (18e)$$

$$v_2^2 = \dot{x}_1^2 + 2l_1\dot{x}_1\dot{\theta}\cos(\beta - \theta) + l_2\dot{x}_1\dot{\theta}_2\cos\theta_2 + l_1^2\dot{\theta}^2 + l_1 l_2\dot{\theta}\dot{\theta}_2[\cos\theta_2\cos(\beta - \theta) - \sin\theta_2\sin(\beta - \theta)] + \frac{l_2^2}{4}\dot{\theta}_2^2 \quad (18f)$$

$$v_3^2 = \dot{X}_{m_3}^2 + \dot{Y}_{m_3}^2 \quad (19a)$$

$$X_{m_3} = x_1 + l_1[\sin\beta - \sin(\beta - \theta)] + l_2\sin\theta_2 + \frac{l_3}{2}\sin\theta_3 \quad (19b)$$

$$\dot{X}_{m_3} = \dot{x}_1 + l_1\dot{\theta}\cos(\beta - \theta) + l_2\dot{\theta}_2\cos\theta_2 + \frac{l_3}{2}\dot{\theta}_3\cos\theta_3 \quad (19c)$$

$$Y_{m_3} = l_1[\cos(\beta - \theta) - \cos\beta)] - l_2(1 - \cos\theta_2) - \frac{l_3}{2}(1 - \cos\theta_3) \quad (19d)$$

$$\dot{Y}_{m_3} = l_1\dot{\theta}\sin(\beta - \theta) - l_2\dot{\theta}_2\sin\theta_2 - \frac{l_3}{2}\dot{\theta}_3\sin\theta_3 \quad (19e)$$

$$v_3^2 = \dot{x}_1^2 + 2l_1\dot{x}_1\dot{\theta}\cos(\beta - \theta) + 2l_2\dot{x}_1\dot{\theta}_2\cos\theta_2 + l_3\dot{x}_1\dot{\theta}_3\cos\theta_3 + l_1^2\dot{\theta}^2 + 2l_1 l_2\dot{\theta}\dot{\theta}_2[\cos\theta_2\cos(\beta - \theta) - \sin\theta_2\sin(\beta - \theta)] + l_1 l_3\dot{\theta}\dot{\theta}_3[\cos\theta_3\cos(\beta - \theta) - \sin\theta_3\sin(\beta - \theta)] + l_2^2\dot{\theta}_2^2 + l_2 l_3\dot{\theta}_2\dot{\theta}_3(\cos\theta_2\cos\theta_3 + \sin\theta_2\sin\theta_3) + \frac{l_3^2}{4}\dot{\theta}_3^2 \quad (19f)$$

where X_{mi} is the resultant longitudinal displacement and Y_{mi} is the resultant vertical displacement (the subscript i denotes the body position where $i = 1$ indicates the lower body, $i = 2$ indicates the middle body and $i = 3$ indicates the upper body), l_1, l_2 and l_3 are the distance from the vehicle's CG to the lower body's CG, the middle-body length and the upper-body length respectively. It is assumed that l_1 is constant owing to the insignificant change in its length during the crash. θ is the pitch angle of the vehicle body and β represents the angle between two lines before any movement of the occupant, where one line is a vertical line from the CG of the vehicle and the other line is connected between the CG of the vehicle and the CG of the occupant's lower body (see Figure 6(c)).

By substituting equations (17f), (18f) and (19f) in equation (16), the kinetic energy can be defined as

$$E = \frac{1}{2}(m_1 + m_2 + m_3)\dot{x}_1^2 + \left[m_1\left(\frac{a^2 + b^2}{24}\right) + (m_1 + m_2 + m_3)l_1^2\right]\dot{\theta}^2 + \left(\frac{m_2}{6} + \frac{m_3}{2}\right)l_2^2\dot{\theta}_2^2 + \frac{m_3}{6}l_3^2\dot{\theta}_3^2 + (m_1 + m_2 + m_3)l_1\dot{x}_1\dot{\theta}\cos(\beta - \theta) + \left(\frac{m_2}{2} + m_3\right)l_2\dot{x}_1\dot{\theta}_2\cos\theta_2 + \frac{m_3}{2}l_3\dot{x}_1\dot{\theta}_3\cos\theta_3 + \left(\frac{m_2}{2} + m_3\right)l_1 l_2\dot{\theta}\dot{\theta}_2\cos(\beta - \theta + \theta_2) + \frac{m_3}{2}l_1 l_3\dot{\theta}\dot{\theta}_3\cos(\beta - \theta + \theta_3) + \frac{m_3}{2}l_2 l_3\dot{\theta}_2\dot{\theta}_3\cos(\theta_2 - \theta_3) \quad (20)$$

The potential energy of the system can be written as

$$V = m_1 g(h + z + Y_{m_1}) + m_2 g\left(h + z + Y_{m_1} + \frac{l_2}{2}\cos\theta_2\right) + m_3 g\left(h + z + Y_{m_1} + l_2\cos\theta_2 + \frac{l_3}{2}\cos\theta_3\right) + \frac{k_1}{2}(\delta_1 - \delta_{s1})^2 + \frac{k_2}{2}(\delta_2 - \delta_{s2})^2 + \frac{k_{R12}}{2}(\theta_2 - \theta)^2 + \frac{k_{R23}}{2}(\theta_3 - \theta_2)^2 \quad (21)$$

where the deflection on the lower seat-belt spring and the deflection on the upper seat-belt spring respectively can be calculated as

$$\delta_1 = x_1 - x \quad (22a)$$

$$\delta_2 = x_1 - x + l_4\sin\theta_2 - l_5[\sin\gamma - \sin(\gamma - \theta)] \quad (22b)$$

where h is the vehicle's CG height. k_1, k_2, k_{R12} and k_{R23} are the lower seat-belt stiffness, the upper seat-belt stiffness, the spring stiffness of pivot 1 and the spring stiffness of pivot 2 respectively. δ_1, δ_2, δ_{s1} and δ_{s2} are the total deflection of the lower seat-belt spring, the total deflection of the upper seat-belt spring, the initial slack length of the lower seat-belt spring and the initial slack length of the upper seat-belt spring respectively. l_4 is the distance between pivot 1 and the contact point between the upper seat-belt spring and the middle body, l_5 is the distance between the vehicle's CG and the contact point between the upper seat-belt spring and the vehicle compartment, and γ is the angle between the line l_5 and vertical centre-line of the vehicle's CG.

The Rayleigh dissipation function can be written as

$$D = \frac{c_1}{2}(\dot{x}_1 - \dot{x})^2 + \frac{c_2}{2}[\dot{x}_1 - \dot{x} + l_4\dot{\theta}_2 \cos\theta_2 - l_5\dot{\theta}\cos(\gamma - \theta)]^2 \tag{23}$$

where c_1 and c_2 are the damping ratio of the lower seat-belt damper and the damping ratio of the upper seat-belt damper respectively.

To obtain the components of equation (15) the differentiations of the kinetic energy, the potential energy and the Rayleigh dissipation function are determined and explained in Appendix 2. Then the different responses x_1, θ_2 and θ_3 of the occupant's bodies can be determined by solving the equations using the central difference method.

Numerical simulations

Primary impact

The mathematical model developed in this investigation is used to study the effect of a VDCS on vehicle collision mitigation. Validation of the vehicle dynamics–crash model was established to determine whether the 3-DOF mathematical model provides a valid measure of vehicle response. This is accomplished by comparing the mathematical model results with real test data[30] and the results of the former ADAMS model.[17] In the real crash test, the vehicle was in free-rolling mode with an impact speed of 16.1 m/s; therefore the same conditions are used in the mathematical model simulation.

The comparison of the mathematical model, the ADAMS multi-body model and the real test results from Transport Research Laboratory data are depicted in Figures 7 and 8. The lower initial speed of 15.1 m/s at the moment of the impact of the ADAMS model as shown in Figure 7 is due to the effect of the rolling resistance prior to impact,[17] while in this paper the initial speed of the mathematical model is adapted to be the same as the actual test impact speed. However, the post-impact velocity curve of the mathematical model is in good correlation with both the real test and the ADAMS model results. The deformation of the front-end structure is illustrated in Figure 8, and a slightly lower value of the maximum deformation appeared in the mathematical model. This may be due to mass differences or other assumed parameters; however, the trends in the three cases are approximately the same. It is clearly shown from this validation of the mathematical model that it is useful and reliable and could be used in many other full-frontal vehicle-to-barrier crash scenarios as presented by the previous work of two of the present authors and a co-worker.[31]

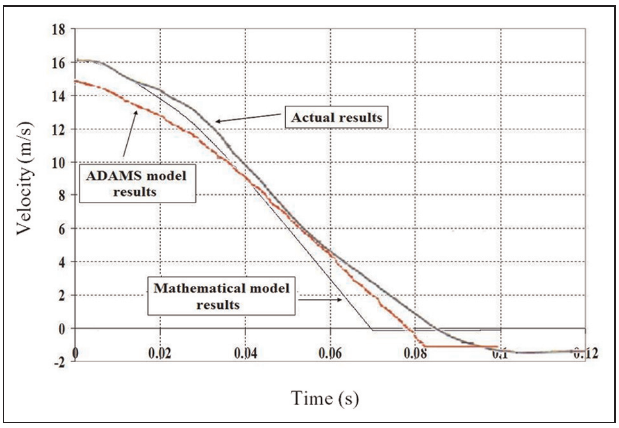

Figure 7. Velocity of the vehicle body.

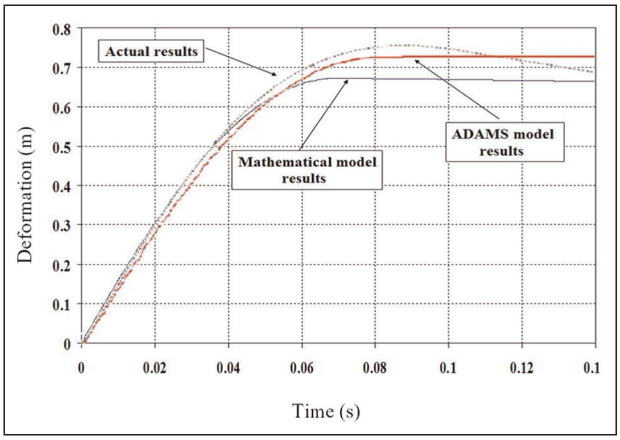

Figure 8. Deformation of the front-end structure.

For vehicle-to-barrier collisions, different crash scenarios were simulated for different VDCSs to investigate their influence on vehicle collision improvement. An ABS control system, an AS control system, an anti-pitch control system and an under-pitch technique were applied and their results were compared with the free-rolling crash scenario. Table 1 introduces the different cases of these active control systems which are used on full-frontal crash scenarios. The values of the different parameters which were used in simulations are as follows: m = 1200 kg; I_{yy} = 1490 kg m^2; k_{Sf} = 36.5 kN/m; k_{Sr} = 27.5 kN/m; c_f = 2200 N s/m; c_r = 1800 N s/m; l_f = 1.185 m; l_r = 1.58 m; h = 0.452 m.

In all cases, the deformation of the front-end structure, the deceleration of the vehicle body, the pitch angle and the acceleration of the vehicle body are determined. While the ADAS detected that the crash will be unavoidable 1.5 s prior to the impact,[3] a VDCS will be applied in this short time preceding the impact. The initial velocities are different in all cases (depending on the active control system), and all velocities will be the same (55 km/h) after 1.5 s when the vehicle reaches the barrier.

Figure 9 shows the deformation–time histories of the front-end structure for all cases. Slight differences in the maximum deformation of the vehicle's front end are found in all the different cases; however, a reduction in the maximum deformation is obtained when the ABS is applied (cases 2 to 5) with almost the same values.

The deceleration–time histories of the vehicle body for all cases are depicted in Figure 10, and it can be

Table 1. Different cases of simulation.

Case	Description
1: Free rolling	The vehicle impacted the barrier without any activated control systems
2: ABS	An ABS is applied
3: ABS + AS	An AS control system is applied together with an ABS
4: ABS + anti-pitch	An anti-pitch control system is applied using the AS components together with an ABS
5: ABS + under-pitch	An under-pitch technique is applied using the AS control system components together with an ABS

ABS: anti-lock braking system; AS: active suspension.

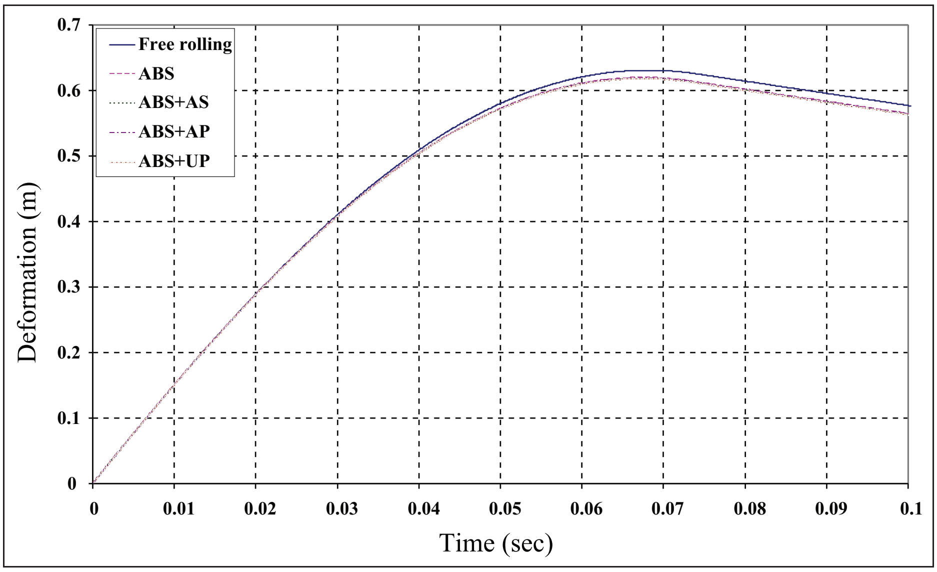

Figure 9. Deformation of the front-end structure for all cases.
ABS: anti-lock braking system; AS: active suspension; AP: anti-pitch; UP: under-pitch.

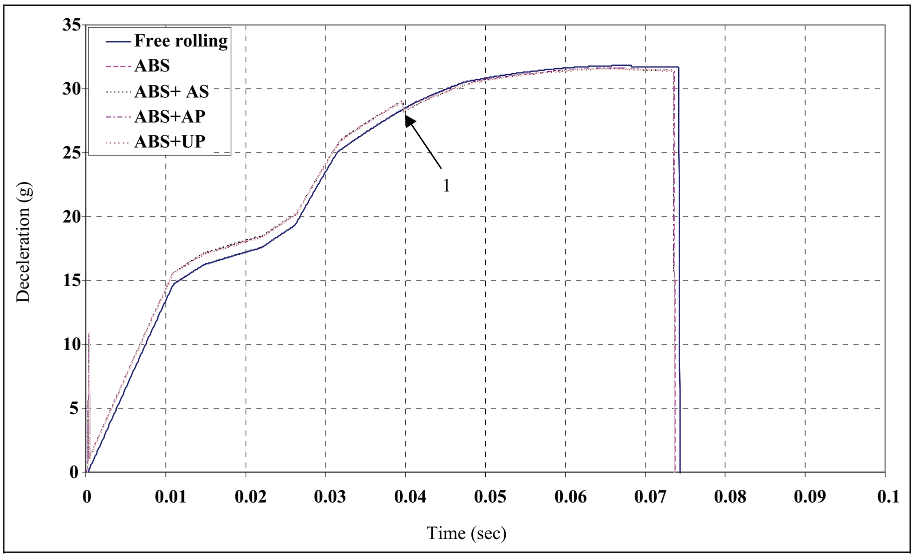

Figure 10. Deceleration of the vehicle body for all cases.
ABS: anti-lock braking system; AS: active suspension; AP: anti-pitch; UP: under-pitch.

said that there is no significant difference in the trends or the values. However, in cases 2 to 5, when the ABS is applied, a very small change in the higher value of the deceleration of the vehicle body is observed in comparison with case 1 (free rolling). These higher values exist until the front wheels reach the barrier and their

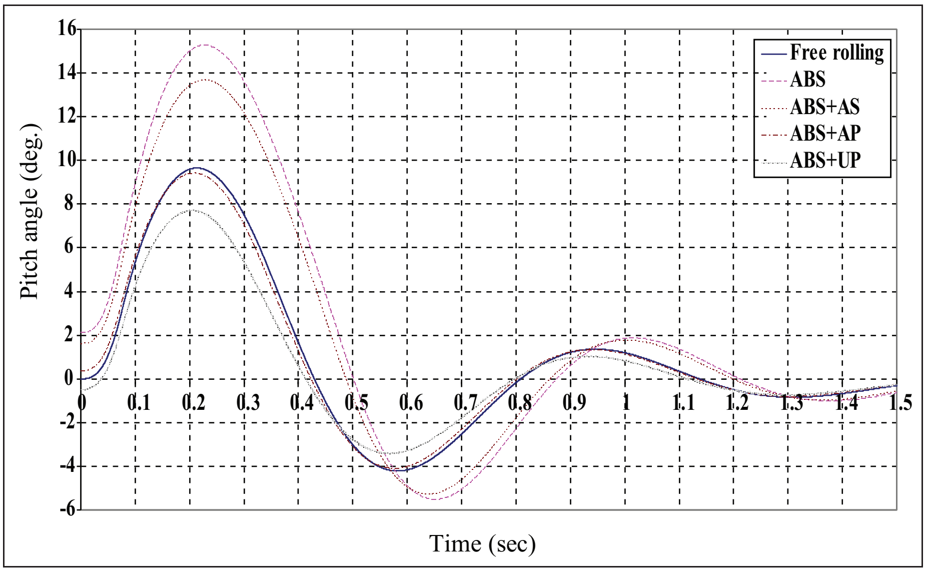

Figure 11. Pitch angle of the vehicle body for all cases.
ABS: anti-lock braking system; AS: active suspension; AP: anti-pitch; UP: under-pitch.

braking effect ends, and a fast reduction in the vehicle body deceleration occurs (arrow 1, Figure 10). At this point, the vehicle body deceleration in case 1 becomes higher than in the other cases, and the maximum value is observed in the case of free rolling.

Figure 11 shows the pitch angle–time histories of the vehicle for all cases. The VDCS is applied 1.5 s before collision and, therefore, the vehicle body impacts the barrier with different pitch angles related to each case, as shown in the figure. The vehicle pitch angle then reaches its maximum values related to each case. Following this, the pitch angle is reduced to reach negative values and then bounces to reach its steady state condition.

The maximum pitch angle is observed in case 2 and this is due to the pitching moment that was generated because of the braking force. In the case of free rolling, the pitch angle of the vehicle body is generated solely because of only the different impact forces between the upper front-end spring and the lower front-end spring. The AS control system is applied together with the ABS to increase the vertical force; therefore, the braking force is increased and the vehicle's stopping distance is decreased.[15] Thus, in case 3, the pitch angle is also large owing to the higher braking force; however, it is smaller than that in case 2 owing to the vertical AS force in the front wheels. In case 4 (ABS + anti-pitch), the anti-pitch control system helps the vehicle to reduce its pitching by generating a pitching moment in the opposite direction, and that clarifies the reduction in the maximum vehicle body pitching in this case, which almost equals the pitch angle in case 1. When the under-pitch technique is applied together with an ABS (case 5), the vehicle is given a negative pitch angle before the impact, and the under-pitch forces will generate a negative pitch moment during the impact. That explains why the maximum pitch angles are lower in case 5.

The pitch acceleration–time histories of the vehicle are depicted in Figure 12 for all three cases. The pitch acceleration increased rapidly to reach its maximum value for each case because of the high pitching moment that is generated from the collision. At the end of the collision, all pitching moments due to the crash equal zero; the vehicle speed is negative with a very small value, and the pitch angle of the vehicle is still positive. This means that the vehicle now is controlled by the tyres and the suspension forces which have already generated a moment in the opposite direction from vehicle pitching. This is the reason for the high drop and the change in direction from positive to negative in the pitch acceleration of the vehicle at the end of the crash. As shown in the figure, the maximum pitch acceleration of the vehicle occurs at the end of the collision and the greatest value of the maximum pitch acceleration is observed in case 2 (ABS) while the lowest value is detected in case 5 (under-pitch technique). Related to this analysis in the full crash scenario, it can be said that the optimum vehicle dynamic control is to apply case 5 (ABS + under-pitch) because the minimum pitch angle and acceleration are obtained in this case.

Secondary impact

The results from the vehicle to a barrier full-frontal crash is taken and used in the occupant's model to obtain the effect of the VDCS on the vehicle's occupant. The following data are used in the numerical simulation:[27] $m_1 = 26.68$ kg; $m_2 = 46.06$ kg; $m_3 = 5.52$ kg; $k_{R12} = 280$ N m/rad; $k_{R23} = 200$ N m/rad; $l_2 = 0.427$ m; $l_3 = 0.24$ m. The total stiffness of the

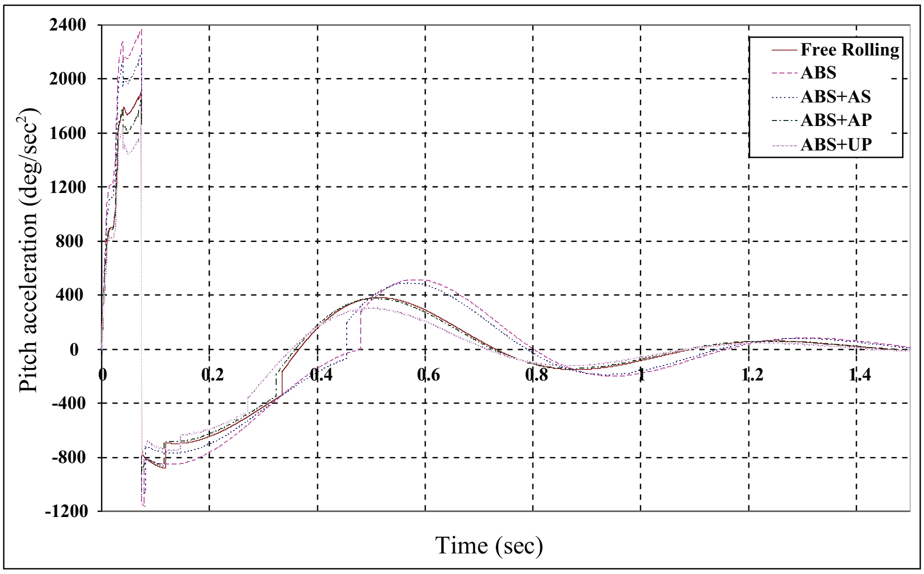

Figure 12. Pitch acceleration of the vehicle body for all cases.
ABS: anti-lock braking system; AS: active suspension; AP: anti-pitch; UP: under-pitch.

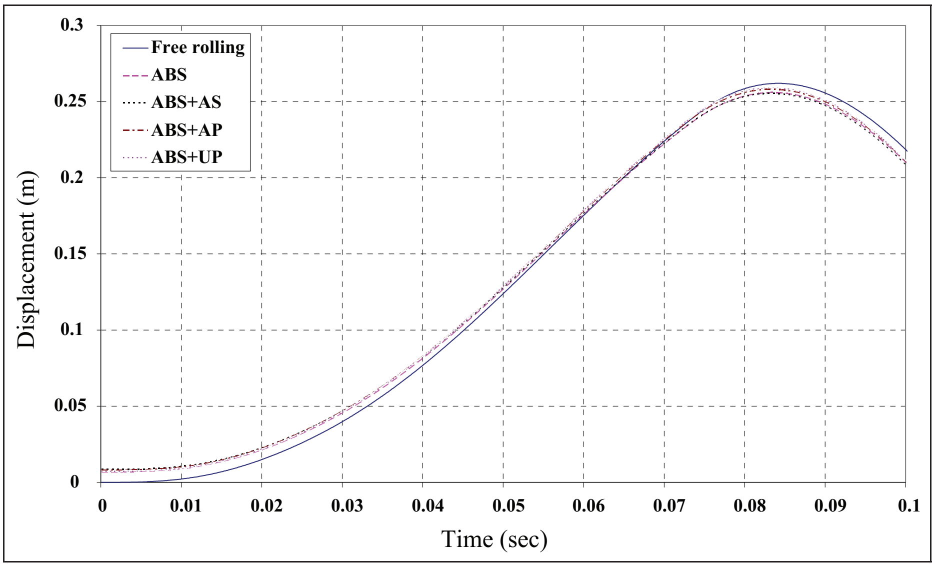

Figure 13. Longitudinal displacement of the occupant's lower body.
ABS: anti-lock braking system; AS: active suspension; AP: anti-pitch; UP: under-pitch.

two seat-belt springs is 98.1 kN/m with a damping coefficient of 20%,[7] and then it is distributed between the upper and lower seat-belt springs in a ratio of 2:3 respectively.[28] $l_1 = 0.3\,\text{m}$, $l_4 = 0.3\,\text{m}$ and $l_5 = 0.35\,\text{m}$ (general assumption ratios). The slack lengths δ_{s1} and δ_{s2} of the seat-belt springs are assumed to be zero.

The longitudinal displacement of the lower body is depicted for all cases in Figure 13; it increases forwards to reach its maximum position and then returns back owing to the seat-belt springs. The maximum displacement is noticed in case 1 (free rolling) while this displacement is slightly decreased in cases 4 and 5, and the minimum displacement is observed in cases 2 and 3. Figure 14 shows the lower-body deceleration for all cases; it increases during the collision to reach its maximum value at the end of impact and then decreases to reach zero value. The sudden decrease in the deceleration (arrow 1 in the figure) is due to the reverse direction of the braking force at the end of impact when the vehicle changes direction and starts to move backwards. It is observed that the maximum deceleration of case 1 is slightly higher than those of the other cases with very small and insignificant values.

The rotation angle of the middle body for all cases is shown in Figure 15, which is quite similar to the pitch angle of the vehicle. The maximum rotation angle is

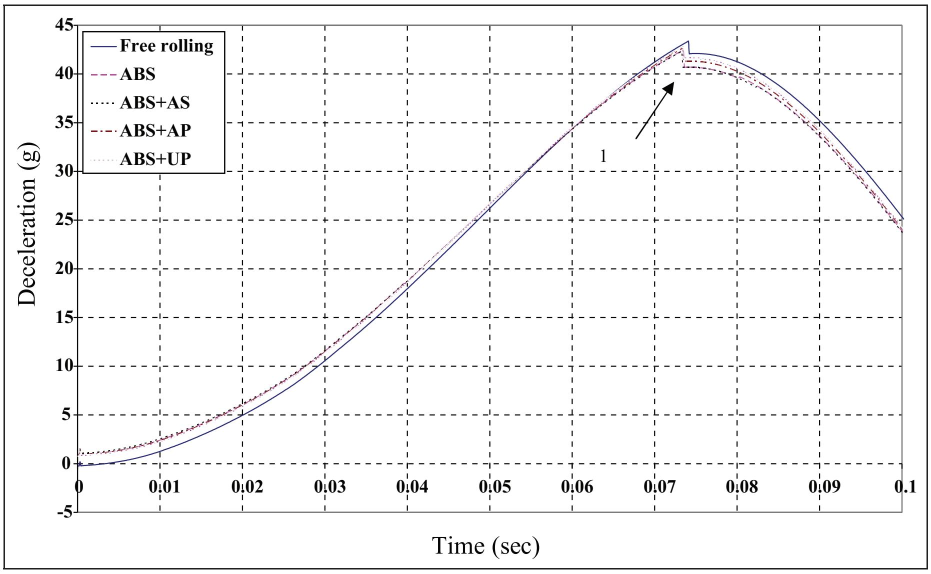

Figure 14. Longitudinal deceleration of the occupant's lower body.
ABS: anti-lock braking system; AS: active suspension; AP: anti-pitch; UP: under-pitch.

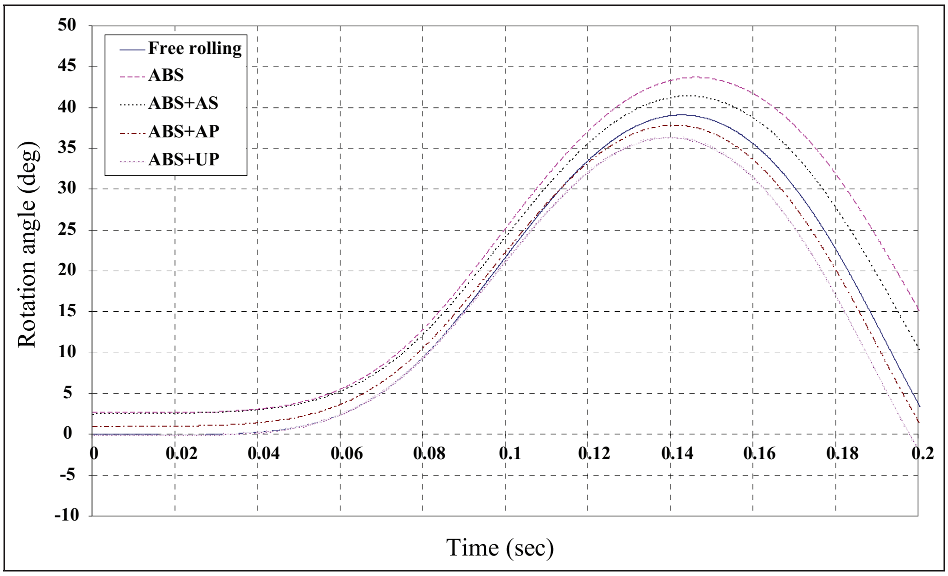

Figure 15. Rotation angle of the occupant's middle body.
ABS: anti-lock braking system; AS: active suspension; AP: anti-pitch; UP: under-pitch.

observed in case 2 (ABS) while the minimum rotation angle is observed in case 5 (ABS + under-pitch). Figure 16 shows the pitch acceleration of the middle body, which is not similar to the pitch acceleration of the vehicle. The maximum pitch acceleration is monitored in case 1 while the minimum pitch acceleration occurred in case 3.

Figure 17 shows the rotation angle of the upper body (head and neck); it is observed from this figure that the maximum rotation angle occurs in case 1 and there is a slight reduction in case 5, while the minimum rotation angle is noticed in the other cases (i.e. cases 2, 3 and 4) with almost the same values. The rotational acceleration of this body is depicted in Figure 18 for all cases; the acceleration starts from different values around zero and then increases to reach its maximum values before the end of impact; after that it decreases to reach its maximum negative values after the end of impact. High values of the maximum positive and negative accelerations are observed in case 1 while the minimum values are noted in case 2, 3 and 4 while the value of acceleration in case 5 has a slightly lower value than in case 1.

The relative rotation angles between the middle body and upper body are given in Figure 19, and the differences between the maximum rotation angles for

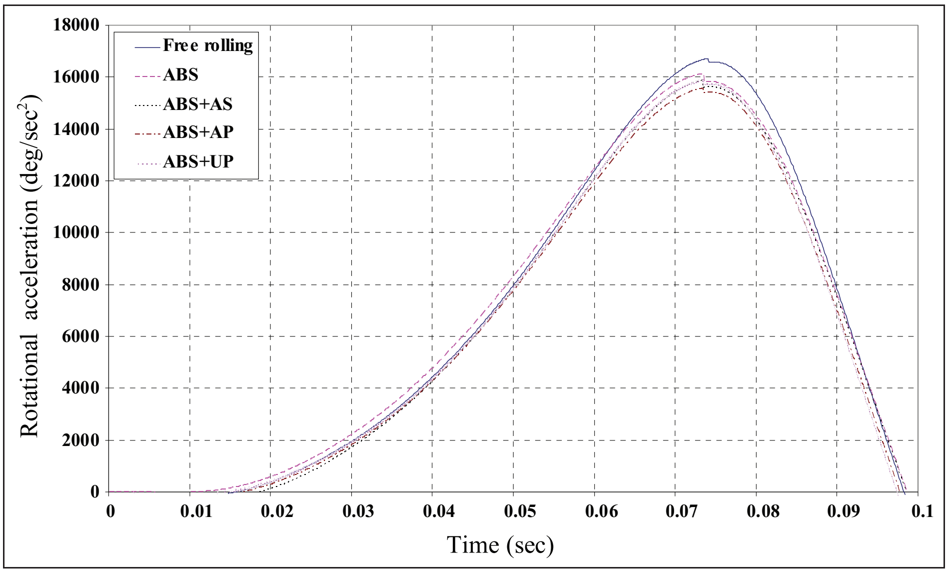

Figure 16. Rotational acceleration of the occupant's middle body.
ABS: anti-lock braking system; AS: active suspension; AP: anti-pitch; UP: under-pitch.

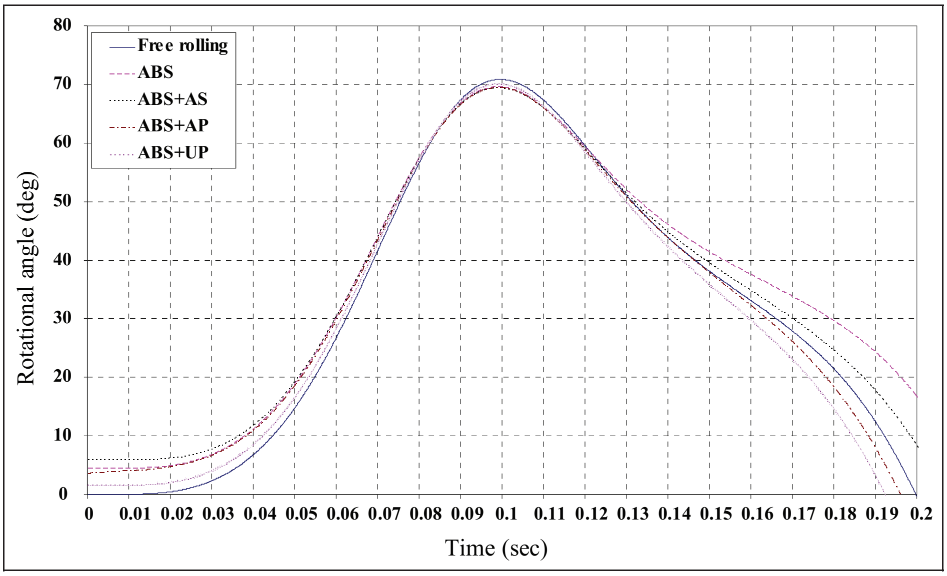

Figure 17. Rotation angle of the occupant's upper body.
ABS: anti-lock braking system; AS: active suspension; AP: anti-pitch; UP: under-pitch.

the different cases in this figure are greater than the differences shown in Figure 17. The maximum rotation angle is observed in cases 1 and 5 while the minimum rotation angles occurred in cases 2 and 3. In case 4 (ABS + anti-pitch) the relative rotation angle decreased in comparison with that in case 1; however, it does not reach the minimum value, as in cases 2 and 3. Figure 20 shows the relative acceleration between the middle body and the upper body, which is quite similar to the rotational acceleration of the upper body in Figure 18. The same results at which the maximum positive and negative accelerations occur are obtained as in case 1, and the minimum positive and negative values are seen in cases 2, 3 and 4 with, of course, different values.

In Figure 21, the horizontal displacement of the upper body is depicted for all cases; this displacement is basically how far the head and neck move forwards in the direction of the steering wheel. The maximum reduction in the head displacement of about 3 cm in case 5 is observed in comparison with the displacement in case 2. Although the overall displacement in each case is greater than the limited space between the occupant's head and the steering wheel, these results are of significance if the restraint system is different (higher seat-belt stiffness) or if an airbag is used in the simulation.

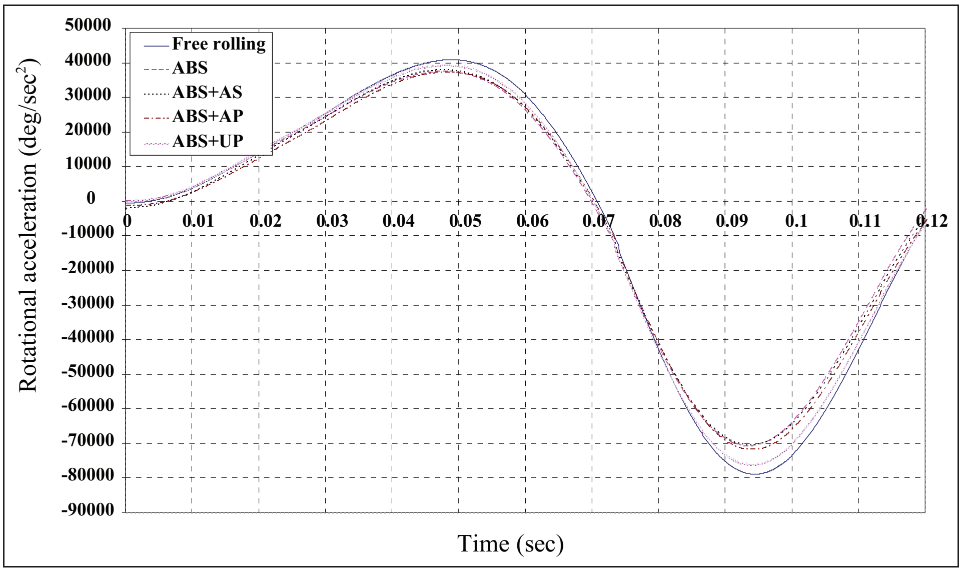

Figure 18. Rotational acceleration of the occupant's upper body.
ABS: anti-lock braking system; AS: active suspension; AP: anti-pitch; UP: under-pitch.

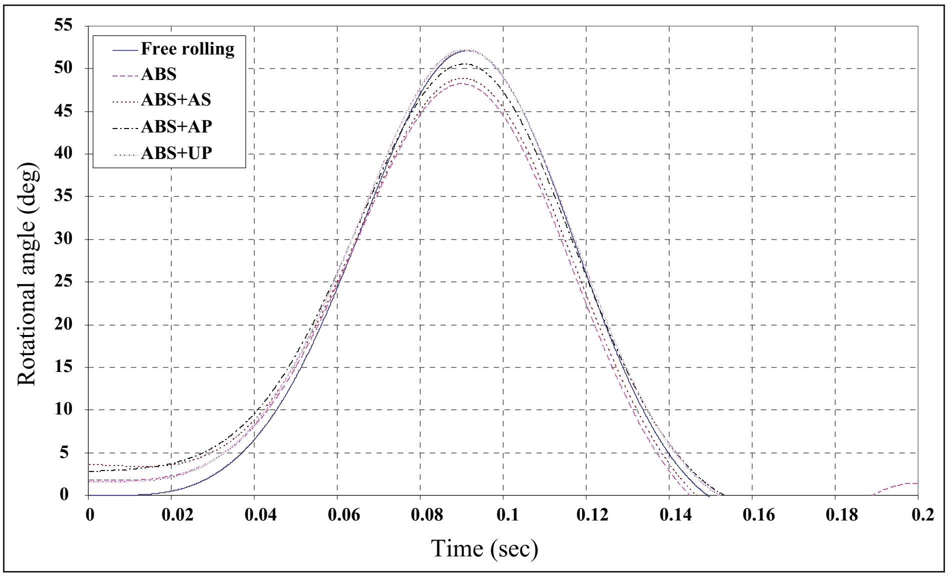

Figure 19. Relative rotation angle θ_3–θ_2.
ABS: anti-lock braking system; AS: active suspension; AP: anti-pitch; UP: under-pitch.

From the above analysis, it can be said that in case 2 (ABS) or case 3 (ABS + AS) the displacement and deceleration of the lower body can be reduced, and the rotation angle and rotational acceleration of the occupant's head can also be decreased. Use of the under-pitch technique (case 5) can help to reduce the rotation angle of the middle body. When the anti-pitch control system is integrated with the ABS (case 4), an improvement in the rotational acceleration of the middle body can be obtained. The VDCS affects the occupant's behaviour in different ways related to the applied case, and it can be seen that the ABS (case 2) can be taken as the best case owing to its effect on the occupant's head (the most important part of the occupant's body). However, further investigations are being carried out to show the effects of the damping of the suspension system of the vehicle and different values for the AS force elements.

Conclusion

A new 3-DOF vehicle dynamics–crash mathematical model and three-mass occupant mathematical model were developed to study the effect of a VDCS on a vehicle crash in a full-frontal vehicle-to-barrier collision. The models presented here would be very useful in the early design stages for assessing the crashworthiness performance of the vehicle and for selecting appropriate

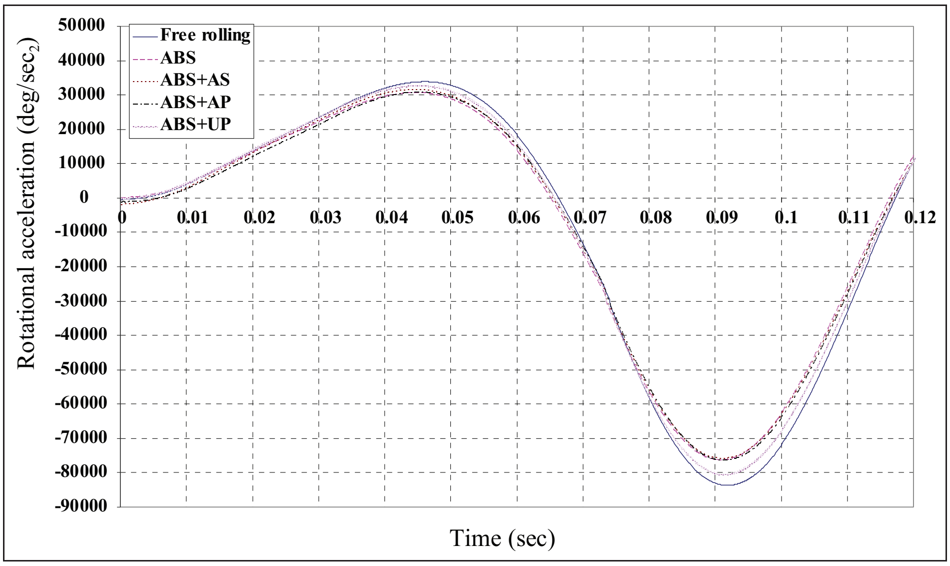

Figure 20. Relative rotational acceleration $\ddot{\theta}_3 - \ddot{\theta}_2$.
ABS: anti-lock braking system; AS: active suspension; AP: anti-pitch; UP: under-pitch.

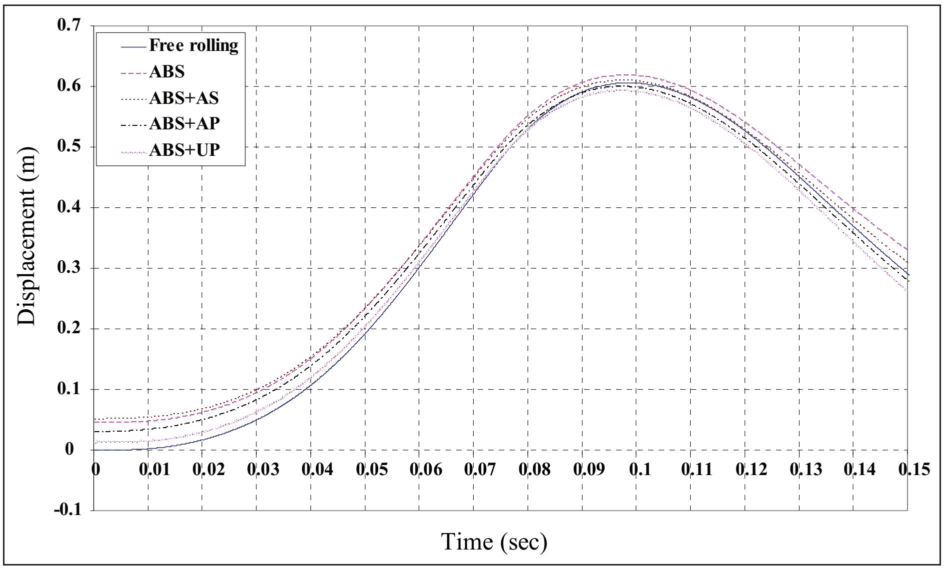

Figure 21. Longitudinal displacement of the occupant's upper body.
ABS: anti-lock braking system; AS: active suspension; AP: anti-pitch; UP: under-pitch.

vehicle parameters. The results obtained for the vehicle deformation and deceleration are reasonably close to those obtained in tests. The results show that the effect of the VDCS is quite minimal in terms of vehicle deformation and deceleration. However, there are significant effects on the vehicle pitching. The VDCS does have a significant effect on the rotations of the middle body and the upper body owing to its effect on the vehicle pitching.

Funding

This work was supported by the Egyptian Government and the Faculty of Engineering, Ain Shams University (grant no. 2004-2/3/56).

Acknowledgement

We acknowledge with sadness the contribution of Professor Dave Crolla who passed away during the period of this research.

References

1. Seiler P, Song B and Hedrick JK. Development of a collision avoidance system. SAE paper 980853, 1998.
2. Tamura M, Inoue H, Watanabe T and Maruko N. Research on a brake assist system with a preview function. SAE paper 2001-01-0357, 2001.
3. Jansson J, Gustafsson F and Johansson J. Decision making for collision avoidance systems. SAE paper 2002-01-0403, 2002.

4. Schoeneburg R and Breitling T. Enhancement of active & passive safety by future pre-safe systems. In: *19th international technical conference on the enhanced safety of vehicles*, Washington, DC, USA, 6–9 June 2005, paper 05-0080-O. Washington, DC: National Highway Traffic Safety Administration.
5. Gietelink O, Ploeg J, De Schutter B and Verhaegen M. Development of advanced driver assistance systems with vehicle hardware-in-the-loop simulations. *Veh System Dynamics* 2006; 44(7): 569–590.
6. Elmarakbi A and Zu J. Mathematical modelling of a vehicle crash with emphasis on the dynamic response analysis of extendable cubic non-linear dampers using the incremental harmonic balance method. *Proc IMechE Part D: J Automobile Engineering* 2007; 221(2): 143–156.
7. Elmarakbi A and Zu J. Dynamic analysis of smart structures for vehicle-to vehicle frontal collision alleviation. *Trans Soc Automot Engrs Japan* 2004; 35: 151–156.
8. Elmarakbi A. Mathematical methodology: incremental harmonic balance method and its application in automotive crashes. SAE paper 2007-01-2140, 2007.
9. Elmarakbi A and Zu J. Incremental harmonic balance method for analysis of standard/smart vehicles-to-rigid barrier frontal collision. *Int J Veh Safety* 2007; 2(3): 288–315.
10. Chang JM, Rahman M, Ali M, et al. Modeling and design for vehicle pitch and drop of body-on-frame vehicles. SAE paper 2005-01-0356, 2005.
11. Chang JM, Ali M, Craig R, et al. Important modeling practices in CAE simulation for vehicle pitch and drop. SAE paper 2006-01-0124, 2006.
12. Chang JM, Huang M, Tyan T, et al. Structural optimization for vehicle pitch and drop. SAE paper 2006-01-0316, 2006.
13. Alleyne A and Hedrick JK. Nonlinear adaptive control of active suspensions. *IEEE Trans Control Systems Technol* 1995; 3(1): 94–102.
14. Yue C, Butsuen T and Hedrick JK. Alternative control laws for automotive active suspensions. *Trans ASME, J Dynamics Systems, Measmt Control* 1989; 111: 286–290.
15. Ting WE and Lin JS. Nonlinear control design of anti-lock braking systems combined with active suspensions. In: *5th Asian control conference*, Melbourne, Australia, 20–23 July 2004, vol. 1, pp.611–616. Piscataway, NJ: IEEE.
16. Mastandrea M and Vangi D. Influence of braking force in low-speed vehicle collisions. *Proc IMechE Part D: J Automobile Engineering* 2005; 219(2): 151–164.
17. Hogan I and Manning W. The use of vehicle dynamic control systems for automotive collision mitigation. In: *3rd Institution of Engineering and Technology conference on automotive electronics*, Warwick, UK, 28–29 June 2007, pp.1–10. Stevenage, Hertfordshire: Institution of Engineering and Technology.
18. Hogan I and Manning W. The development of a vehicle collision mitigation control system through multibody modelling. In: *32nd FISITA world automotive congress*, Munich, Germany, 14–19 September 2008, paper F2008-08-055. London: FISITA.
19. Hogan I. *The use of vehicle dynamic control systems for automotive collision mitigation*. PhD Thesis, Department of Engineering and Technology, Manchester Metropolitan University, Manchester, UK, 2008.
20. Emori RI. Analytical approach to automobile collisions. SAE paper 680016, 1968.
21 Kamal MM. Analysis and simulation of vehicle to barrier impact. SAE paper 700414, 1970.
22. Khattab A. *Investigation of an adaptable crash energy management system to enhance vehicle crashworthiness*. PhD Thesis, Department of Mechanical and Industrial Engineering, Concordia University, Canada, 2010.
23. Pennestrì E, Valentini PP and Vita L. Comfort analysis of car occupants: comparison between multibody and finite element models. *Int J Veh Systems Modelling Testing* 2005; 1(1–3): 68–78.
24. Zhang H, Parenteau CS, Katta D and Raman SV. Applications of human body model in a vehicle environment. In: *9th International MADYMO User Conference*, Como, Italy, 10–11 October 2002. Como: TNO Automotive.
25. Renneker DN. A basic study of 'energy-absorbing' vehicle structure and occupant restraints by mathematical model. SAE paper 670897, 1967.
26. Weaver JR. A simple occupant dynamics model. *J Biomech* 1968; 1(3): 185–191.
27. Ilie S and Tabacu S. Study of the occupant's kinematics during the frontal impact. *Ann Oradea Univ, Fascicle Managmt Technol Engng* 2007; 6(16): 542–551.
28. Paulitz TJ, Blackketter DM and Rink KK. Constant force restraints for frontal collisions. *Proc IMechE Part D: J Automobile Engineering* 2006; 220(9): 1177–1189.
29. Roberts VL and Robins DH. Multidimensional mathematical modeling of occupant dynamics under crash conditions. SAE paper 690248, 1969.
30. Transport Research Laborotory. Adaptive vehicle structures for secondary safety, http://www.transportresearchfoundation.co.uk/PDF/Adaptive%20vehicle%20structures%20for% 20secondary%20safety_PPR310.PDF (1995).
31. Elkady M, Elmarakbi A, and Crolla D. A new mathematical model to study the influence of vehicle dynamics control on vehicle collision. In: *33rd FISITA world automotive congress*, Budapest, Hungary, 30 May–4 June 2010, paper F2010-C-113. London: FISITA.

Appendix 1

Notation

c	damping coefficient of the suspension spring
c_1	damping ratio of the lower seat-belt damper
c_2	damping ratio of the upper seat-belt damper
D	Rayleigh dissipation function of the system
e_1	distance between the centre of gravity of the vehicle body and the upper front-end springs
e_2	distance between the centre of gravity of the vehicle body and the lower front-end springs
E	kinetic energy of the system
F	constant
F_b	braking force

F_s front-end spring force
F_S suspension force
F_z vertical normal force on the tyres
g acceleration due to gravity
h distance between the centre of gravity of the vehicle body and the road
I_1, I_2, I_3 rotational moments of inertia of the first body, the second body and the third body respectively of the occupant
I_{yy} moment of inertia of the vehicle body about the y axis
k_{R12} spring stiffness of pivot 1
k_{R23} spring stiffness of pivot 2
k_s front-end spring stiffness
k_S suspension spring stiffness
k_1 lower seat-belt stiffness
k_2 upper seat-belt stiffness
l wheelbase of the vehicle
l_f distance between the centre of gravity of the vehicle body and the front wheels
l_r distance between the centre of gravity of the vehicle body and the rear wheels
l_1 distance from the centre of gravity of the vehicle to the centre of gravity of the lower body of the occupant
l_2 occupant's middle-body length
l_3 occupant's upper-body length
l_4 distance between pivot 1 and the contact point between the upper seat-belt spring and the occupant's middle body
l_5 distance between the centre of gravity of the vehicle and the contact point between the upper seat-belt spring and the vehicle compartment
m mass of the vehicle body
m_1, m_2, m_3 masses of the lower body, the middle body and the upper body respectively of the occupant
u active force element
v_1, v_2, v_3 equivalent velocities of the lower body, the middle body and the upper body respectively of the occupant
V potential energy of the system
x longitudinal position of the centre of gravity of the vehicle
$\ddot{x}$ acceleration of the vehicle body in the longitudinal direction
x_1, $\dot{x}_1$, $\ddot{x}_1$ longitudinal movement, velocity and acceleration respectively of the occupant's lower body
X_{m1}, X_{m2}, X_{m3} resultant longitudinal displacements of the lower body, the middle body and the upper body respectively of the occupant
Y_{m1}, Y_{m2}, Y_{m3} resultant vertical displacements of the lower body, the middle body and the upper body respectively of the occupant
z vertical position of the centre of gravity of the vehicle
$\dot{z}$ velocity of the vehicle body in the vertical direction
$\ddot{z}$ acceleration of the vehicle body in the vertical direction
β angle between the vertical centre-line of the vehicle and the line between the centre of gravity of the vehicle and the centre of gravity of the occupant's lower body
γ angle between the line l_5 and vertical centre-line of the centre of gravity of the vehicle
δ deformation of the front-end spring
δ_{s1} initial slack length of the lower seat-belt spring
δ_{s2} initial slack length of the upper seat-belt spring
δ_1 total deflection of the lower seat-belt spring
δ_2 total deflection of the upper seat-belt spring
θ, $\dot{\theta}$, $\ddot{\theta}$ pitch angle, pitch angular velocity and pitch rotational acceleration respectively about the centre of gravity of the vehicle body
θ_2, $\dot{\theta}_2$, $\ddot{\theta}_2$ rotation angle, rotational velocity and rotational acceleration respectively of the occupant's middle body
θ_3, $\dot{\theta}_3$, $\ddot{\theta}_3$ rotation angle, rotational velocity and rotational acceleration respectively of the occupant's upper body
λ tyre slip ratio
μ friction coefficient between the tyre and the road

Subscripts

f front wheels
i spring location ($i = u$ indicates upper springs; $i = l$ indicates lower springs)
j different stages of the force–deformation characteristics (see Figure 3)
l lower front-end springs
r rear wheels
u upper front-end springs

Appendix 2

In this appendix the differentiation of the kinetic energy, the potential energy and the Rayleigh dissipation function are performed related to equation (15) according to

$$\begin{aligned}\frac{\mathrm{d}}{\mathrm{d}t}\left(\frac{\partial E}{\partial \dot{x}_1}\right) &= (m_1+m_2+m_3)\ddot{x}_1+(m_1+m_2+m_3)\\ &\quad l_1[\ddot{\theta}\cos(\beta-\theta)+\dot{\theta}^2\sin(\beta-\theta)]\\ &\quad +\left(\frac{m_2}{2}+m_3\right)l_2(\ddot{\theta}_2\cos\theta_2-\dot{\theta}_2^2\sin\theta_2)\\ &\quad +\frac{m_3}{2}l_3(\ddot{\theta}_3\cos\theta_3-\dot{\theta}_3^2\sin\theta_3)\end{aligned} \tag{24a}$$

$$\begin{aligned}\frac{\mathrm{d}}{\mathrm{d}t}\left(\frac{\partial E}{\partial \dot{\theta}_2}\right) &= \left(\frac{m_2}{3}+m_3\right)l_2^2\ddot{\theta}_2+\left(\frac{m_2}{2}+m_3\right)\\ &\quad l_2(\ddot{x}_1\cos\theta_2-\dot{x}_1\dot{\theta}_2\sin\theta_2)\\ &\quad +\left(\frac{m_2}{2}+m_3\right)l_1l_2[\ddot{\theta}\cos(\beta-\theta+\theta_2)\\ &\quad -\dot{\theta}(\dot{\theta}_2-\dot{\theta})\sin(\beta-\theta+\theta_2)]\\ &\quad +\frac{m_3}{2}l_2l_3[(\ddot{\theta}_3\cos(\theta_2-\theta_3)\\ &\quad -\dot{\theta}_3(\dot{\theta}_2-\dot{\theta}_3)\sin(\theta_2-\theta_3)]\end{aligned} \tag{24b}$$

$$\begin{aligned}\frac{\mathrm{d}}{\mathrm{d}t}\left(\frac{\partial E}{\partial \dot{\theta}_3}\right) &= \frac{m_3}{3}l_3^2\ddot{\theta}_3+\frac{m_3}{2}l_3(\ddot{x}_1\cos\theta_3-\dot{x}_1\dot{\theta}_3\sin\theta_3)\\ &\quad +\frac{m_3}{2}l_1l_3[\ddot{\theta}\cos(\beta-\theta+\theta_3)\\ &\quad -\dot{\theta}(\dot{\theta}_3-\dot{\theta})\sin(\beta-\theta+\theta_3)]\\ &\quad +\frac{m_3}{2}l_2l_3[\ddot{\theta}_2\cos(\theta_2-\theta_3)\\ &\quad -\dot{\theta}_2(\dot{\theta}_2-\dot{\theta}_3)\sin(\theta_2-\theta_3)]\end{aligned} \tag{24c}$$

$$\frac{\partial E}{\partial x_1}=0 \tag{24d}$$

$$\begin{aligned}\frac{\partial E}{\partial \theta_2} &= -\left(\frac{m_2}{2}+m_3\right)l_2\dot{x}_1\dot{\theta}_2\sin\theta_2\\ &\quad -\left(\frac{m_2}{2}+m_3\right)l_1l_2\dot{\theta}\dot{\theta}_2\sin(\beta-\theta+\theta_2)\\ &\quad -\frac{m_3}{2}l_2l_3\dot{\theta}_2\dot{\theta}_3\sin(\theta_2-\theta_3)\end{aligned} \tag{24e}$$

$$\begin{aligned}\frac{\partial E}{\partial \theta_3} &= -\frac{m_3}{2}l_3\dot{x}_1\dot{\theta}_3\sin\theta_3\\ &\quad -\frac{m_3}{2}l_1l_3\dot{\theta}\dot{\theta}_3\sin(\beta-\theta+\theta_3)\\ &\quad +\frac{m_3}{2}l_2l_3\dot{\theta}_2\dot{\theta}_3\sin(\theta_2-\theta_3)\end{aligned} \tag{24f}$$

$$\begin{aligned}\frac{\partial V}{\partial x_1} &= k_1(x_1-x-\delta_{s1})\\ &\quad +k_2\{x_1-x+l_4\sin\theta_2\\ &\quad -l_5[\sin\gamma-\sin(\gamma-\theta)]-\delta_{s2}\}\end{aligned} \tag{24g}$$

$$\begin{aligned}\frac{\partial V}{\partial \theta_2} &= -m_2g\frac{l_2}{2}\sin\theta_2-m_3gl_2\sin\theta_2\\ &\quad +k_2l_4\cos\theta_2\{x_1-x+l_4\sin\theta_2\\ &\quad -l_5[\sin\gamma-\sin(\gamma-\theta)]-\delta_{s2}\}\\ &\quad +k_{R12}(\theta_2-\theta)-k_{R23}(\theta_3-\theta_2)\end{aligned} \tag{24h}$$

$$\frac{\partial V}{\partial \theta_3} = -\frac{m_3}{2}gl_3\sin\theta_3+k_{R23}(\theta_3-\theta_2) \tag{24i}$$

$$\begin{aligned}\frac{\partial D}{\partial \dot{x}_1} &= c_1(\dot{x}_1-\dot{x})+c_2[\dot{x}_1-\dot{x}+l_4\dot{\theta}_2\cos\theta_2\\ &\quad -l_5\dot{\theta}\cos(\gamma-\theta)]\end{aligned} \tag{24j}$$

$$\begin{aligned}\frac{\partial D}{\partial \dot{\theta}_2} &= c_2l_4\cos\theta_2[\dot{x}_1-\dot{x}\\ &\quad +l_4\dot{\theta}_2\cos\theta_2-l_5\dot{\theta}\cos(\gamma-\theta)]\end{aligned} \tag{24k}$$

$$\frac{\partial D}{\partial \dot{\theta}_3}=0 \tag{24l}$$

By substituting the components of equations (24) into equation (15), the final forms of the equations of motion become

$$a_{11}\ddot{x}_1+a_{12}\ddot{\theta}_2+a_{13}\ddot{\theta}_3=f_1(x_1,\theta_2,\theta_3,\dot{x}_1,\dot{\theta}_2,\dot{\theta}_3) \tag{25a}$$

$$a_{21}\ddot{x}_1+a_{22}\ddot{\theta}_2+a_{23}\ddot{\theta}_3=f_2(x_1,\theta_2,\theta_3,\dot{x}_1,\dot{\theta}_2,\dot{\theta}_3) \tag{25b}$$

$$a_{31}\ddot{x}_1+a_{32}\ddot{\theta}_2+a_{33}\ddot{\theta}_3=f_3(x_1,\theta_2,\theta_3,\dot{x}_1,\dot{\theta}_2,\dot{\theta}_3) \tag{25c}$$

The system then can be written in the matrix form as

$$[A][\ddot{B}]=[F] \tag{26a}$$

where

$$[A]=\begin{bmatrix} m_1+m_2+m_3 & \left(\frac{m_2}{2}+m_3\right)l_2\cos\theta_2 & \frac{m_3}{2}l_3\cos\theta_3\\ \left(\frac{m_2}{2}+m_3\right)l_2\cos\theta_2 & \left(\frac{m_2}{3}+m_3\right)l_2^2 & \frac{m_3}{2}l_2l_3\cos(\theta_2-\theta_3)\\ \frac{m_3}{2}l_3\cos\theta_3 & \frac{m_3}{2}l_2l_3\cos(\theta_2-\theta_3) & \frac{m_3}{3}l_3^2\end{bmatrix} \tag{26b}$$

$$[\ddot{B}]=\begin{bmatrix}\ddot{x}_1\\ \ddot{\theta}_2\\ \ddot{\theta}_3\end{bmatrix} \tag{26c}$$

$$[F]=\begin{bmatrix}f_{11}\\ f_{12}\\ f_{13}\end{bmatrix} \tag{26d}$$

where

$$\begin{aligned}f_{11} &= -(m_1+m_2+m_3)l_1[\ddot{\theta}\cos(\beta-\theta)\\ &\quad +\dot{\theta}^2\sin(\beta-\theta)]+\left(\frac{m_3}{2}+m_3\right)l_2\dot{\theta}_2^2\sin\theta_2\\ &\quad +\frac{m_3}{2}l_3\dot{\theta}_3^2\sin\theta_3-k_1(x_1-x-\delta_{s1})\\ &\quad -k_2\{x_1-x+l_4\sin\theta_2\\ &\quad -l_5[\sin\gamma-\sin(\gamma-\theta)]-\delta_{s2}\}\\ &\quad -c_1(\dot{x}_1-\dot{x})-c_2[\dot{x}_1-\dot{x}+l_4\dot{\theta}_2\cos\theta_2\\ &\quad -l_5\dot{\theta}\cos(\gamma-\theta)]\end{aligned} \tag{26e}$$

$$\begin{aligned}f_{12} &= -\left(\frac{m_2}{2}+m_3\right)l_1l_2[\ddot{\theta}\cos(\beta-\theta+\theta_2)\\ &\quad -\dot{\theta}(\dot{\theta}_2-\dot{\theta})\sin(\beta-\theta+\theta_2)]\end{aligned}$$

$$
\begin{aligned}
&+\frac{m_3}{2} l_2 l_3 \dot{\theta}_3^2 \sin(\theta_2-\theta_3)\\
&-\left(\frac{m_2}{2}+m_3\right) l_1 l_2 \dot{\theta}\dot{\theta}_2 \sin(\beta-\theta+\theta_2)\\
&+\left(\frac{m_2}{2}+m_3\right) g l_2 \sin\theta_2\\
&-k_2 l_4 \cos\theta_2 \{x_1 - x + l_4 \sin\theta_2\\
&-l_5[\sin\gamma - \sin(\gamma-\theta)] - \delta_{s2}\}\\
&-k_{R12}(\theta_2-\theta) - k_{R23}(\theta_3-\theta_2)\\
&-c_2 l_4 \cos\theta_2 [\dot{x}_1 - \dot{x} + l_4 \dot{\theta}_2 \cos\theta_2\\
&-l_5 \dot{\theta} \cos(\gamma-\theta)]
\end{aligned}
\tag{26f}
$$

$$
\begin{aligned}
f_{13} = &-\frac{m_3}{2} l_1 l_3 [\ddot{\theta} \cos(\beta-\theta+\theta_3)\\
&-\dot{\theta}(\dot{\theta}_3-\dot{\theta}) \sin(\beta-\theta+\theta_3)]\\
&+\frac{m_3}{2} l_2 l_3 \dot{\theta}_2^2 \sin(\theta_2-\theta_3)\\
&-\frac{m_3}{2} l_1 l_3 \dot{\theta}\dot{\theta}_3 \sin(\beta-\theta+\theta_3)\\
&+\frac{m_3}{2} g l_3 \sin\theta_3 - k_{R23}(\theta_3-\theta_2)
\end{aligned}
\tag{26g}
$$

Then the final equations of motions of the system can be written as

$$
[\ddot{B}] = [A]^{-1}[F] \tag{27}
$$

Therefore the different occupant's bodies responses x_1, θ_2 and θ_3 can be determined by solving equation (27) using the central difference method.